

Article

Effects of Erucamide and N-phenyl- α -naphthylamine on the Friction and Torque Behaviors of Grease on Roller Bearings

Qingchun Liu ^{1,*} , Yimin Mo ¹, Juncheng Lv ^{1,2} and Hong Zhang ^{1,2} 

¹ School of Mechanical and Electronic Engineering, Wuhan University of Technology, 122 Luoshi Road, Wuhan 430070, China; moyimin@whut.edu.cn (Y.M.); juncheng.lv@sgmw.com.cn (J.L.); hongybyb@163.com (H.Z.)

² SAIC GM Wuling Automobile Co., Ltd., 18 Hexi Road, Liuzhou 545007, China

* Correspondence: liuqingchun369@163.com

Abstract: To evaluate the impact of various proportions of erucamide and N-phenyl- α -naphthylamine on grease's tribological performance for roller bearings, lithium complex grease (LCG) and polyurea grease (PG) were prepared with erucamide and N-phenyl- α -naphthylamine proportions of (0,0), (0,3), (1,2), (2,1), and (3,0). An investigation was conducted into the microscopic structures of the ten greases and their effects on the friction coefficients and wear scars of GCr15 steel. These findings were validated through bearing friction torque tests. The results indicate that the addition of 2 wt. % erucamide and 1 wt. % N-phenyl- α -naphthylamine to PG/LCG significantly enhances their tribological properties and reduces friction torque, with PG exhibiting superior performance. This enhancement was attributed to the synergistic interaction of erucamide and N-phenyl- α -naphthylamine with the lamellar thickener within PG. Erucamide contributed to friction reduction, while N acted as an antioxidant.

Keywords: erucamide; N-phenyl- α -naphthylamine; friction torque; friction and wear



Citation: Liu, Q.; Mo, Y.; Lv, J.; Zhang, H. Effects of Erucamide and N-phenyl- α -naphthylamine on the Friction and Torque Behaviors of Grease on Roller Bearings. *Lubricants* **2023**, *11*, 531. <https://doi.org/10.3390/lubricants11120531>

Received: 20 November 2023

Revised: 9 December 2023

Accepted: 12 December 2023

Published: 14 December 2023



Copyright: © 2023 by the authors. Licensee MDPI, Basel, Switzerland. This article is an open access article distributed under the terms and conditions of the Creative Commons Attribution (CC BY) license (<https://creativecommons.org/licenses/by/4.0/>).

1. Introduction

The friction torque of bearings, including both the starting torque and dynamic torque, exerts a direct influence on the transmission efficiency, life, and stability of automotive transmission systems. It stands as a pivotal metric for the evaluation of bearing performance [1–5]. With the progressively stringent nature of automotive standards, roller bearings, integral components of automobiles, necessitate continual refinement. Grease, an indispensable constituent of bearings, has emerged as an important factor impacting bearing performance [6,7]. To enhance the tribological properties of grease and mitigate the attributes of friction torque of bearings, numerous researchers have dedicated their efforts to the quest for superior base oils and thickeners [8–10]. Such endeavors result in the reduction in frictional wear and friction torque in roller bearings, thereby enhancing the transmission efficiency and stability of automotive transmission systems while concurrently extending their operational lifespan.

In recent years, researchers have explored the tribological phenomena of additives in greases [9,11,12]. Bas H et al. [13] analyzed friction and wear by adding MoS₂ and CaF₂ additives to lithium soap grease. The results revealed that the MoS₂ and CaF₂ additives can improve the wear resistance of lithium grease and reduce the friction coefficient. Padgurskas J et al. [14] used rapeseed oil as a base oil and beeswax as a thickener, adding functional anti-wear and antioxidant additives and carbon nanoparticles of graphene oxide to modify the grease, and the results showed that functional additives and nanoparticles significantly improve tribological properties and reduce the wear rate. Wang YS et al. [10] selected Molybdenum dialkyl dithiophosphate (MoDDP) and potassium borate (PB) as additives for greases. The results showed that due to the combined effect, the PB/MoDDP additive combination can achieve excellent friction reduction and anti-wear performance. In addition to the aforementioned references, various other additives, such as molybdenum

disulfide (MoS₂) [15], zinc dialkyl dithiophosphate (ZDDP) [16], and polytetrafluoroethylene (PTFE) [17], have been explored for enhancing the physicochemical properties of grease. However, it is essential to acknowledge that the frictional behaviors in roller bearings, including ball rolling and sliding between the cage and inner and outer rings, cannot be solely evaluated based on the friction and wear performance of the grease. Hence, it is imperative to integrate grease into the overall roller bearing system and conduct a more comprehensive study and validation of its tribological performance on roller bearings.

As polymer development has advanced, erucamide has garnered extensive attention due to its outstanding tribological properties [18–20]. Jia TY et al. [21] used erucamide as a lubricant to melt blended with thermoplastic polyurethane (TPU) to reduce the friction coefficient of TPU, thereby improving the wearing comfort of intelligent wearable devices. Velázquez JDH et al. [22] linked erucamide to the graphene sheet and found that erucamide chains tend to remain closer together through pi–pi stacking interactions arising from the double bonds located at C₁₃–C₁₄, and that this arrangement of erucamide chains was responsible for the lower friction coefficient of erucamide brushes, which was a macroscopic consequence of cooperative quantum mechanical interactions. Di YY et al. [23] added erucamide to a self-assembled film (SAF) to prepare erucamide SAFs. When erucamide was laid on the surface of the SAF, it showed obvious atomic stick–slip friction behavior and ultra-low frictional dissipation. The friction–reduction and lubrication performance of erucamide are determined by its rheological characteristics and the interplay between its molecular structure; thus, studying the molecular structure and arrangement of erucamide is of the utmost importance [24,25]. The structure of erucamide comprises circular head clusters and outwardly extending hydrophobic tail ends. These arrangements are placed between the friction pairs, preventing direct contact between the friction surfaces and thereby converting sliding friction into rolling friction, thereby enhancing the friction wear performance. Currently, research on erucamide primarily focuses on its antifriction properties with polymers, with limited discussion regarding its application within greases. As a novel grease additive, it has shown the potential to exhibit excellent tribological performance [26].

With the evolution of greases, researchers have observed that base oils are susceptible to oxidation, polymerization, and degradation [27,28]. Therefore, it is imperative to incorporate antioxidants into greases to mitigate and reduce base oil oxidation. Common antioxidants in greases include dioctyldiphenylamine (DODPA) [29], diphenylamine [30,31], and N-phenyl- α -naphthylamine [32,33]. Compared to other antioxidants, N-phenyl- α -naphthylamine could synergistically interact with anti-wear agents, and it exhibited excellent anti-wear and load-carrying properties, as well as high antioxidative characteristics [34,35]. However, the synergistic mechanisms of erucamide as an anti-wear agent and N-phenyl- α -naphthylamine as an antioxidant, as well as the role of erucamide and N-phenyl- α -naphthylamine in different thickener structures, need to be studied. These aspects are pivotal for the synergistic lubrication of erucamide, N-phenyl- α -naphthylamine, and greases.

In summary, two typical grease types, namely polyurea grease and lithium complex grease, were selected. Various proportions of the additives erucamide and N-phenyl- α -naphthylamine were added into these two types of grease, and their friction and wear performance, as well as lubrication mechanisms, were studied. Roller bearing friction torque tests were conducted to investigate and validate the impact of the greases containing various proportions of erucamide and N-phenyl- α -naphthylamine on the frictional properties of roller bearings. This study could provide the experimental basis for the application of erucamide and N-phenyl- α -naphthylamine in GCr15 bearings to achieve excellent antifriction and wear resistance performances.

2. Materials and Methods

2.1. Selection of Base Oil

This study utilized the same base oil for the preparation of greases. The chosen base oil was polyalphaolefin mineral oil (PAO4), supplied by Sinopec. The key properties of the base oil are summarized in Table 1. PAO4 exhibits favorable kinematic viscosity, which aids in the formation of oil film.

Table 1. Key properties of base oil.

Project	PAO4	Test Method
Kinematic viscosity (40 °C)/(mm ² ·s ⁻¹)	19.063	GB/T 265
Kinematic viscosity (100 °C)/(mm ² ·s ⁻¹)	6.342	GB/T 265

2.2. Preparation of Grease

2.2.1. Preparation of Polyurea Grease

Polyurea grease was prepared through a high-temperature blending process of methylene diphenyl diisocyanate (MDI) and cyclohexylamine in base oil, as depicted in Figure 1a. A flow chart of the polyurea grease preparation process is shown in Figure 2a. The specific preparation procedure was divided into five steps:

- MDI and cyclohexylamine were individually dissolved in the base oil and continuously stirred to obtain two mixed solutions.
- The temperature of the reactor was set to 100 °C, and the two mixed solutions were introduced into the reactor for 30 min. During this process, a suitable amount of distilled water was added to remove excess MDI.
- The reactor temperature was set to 150 °C and maintained for 30 min.
- The temperature of the reactor was reduced to room temperature.
- The mixture was poured into a three-roller grinder for grinding to obtain PG.

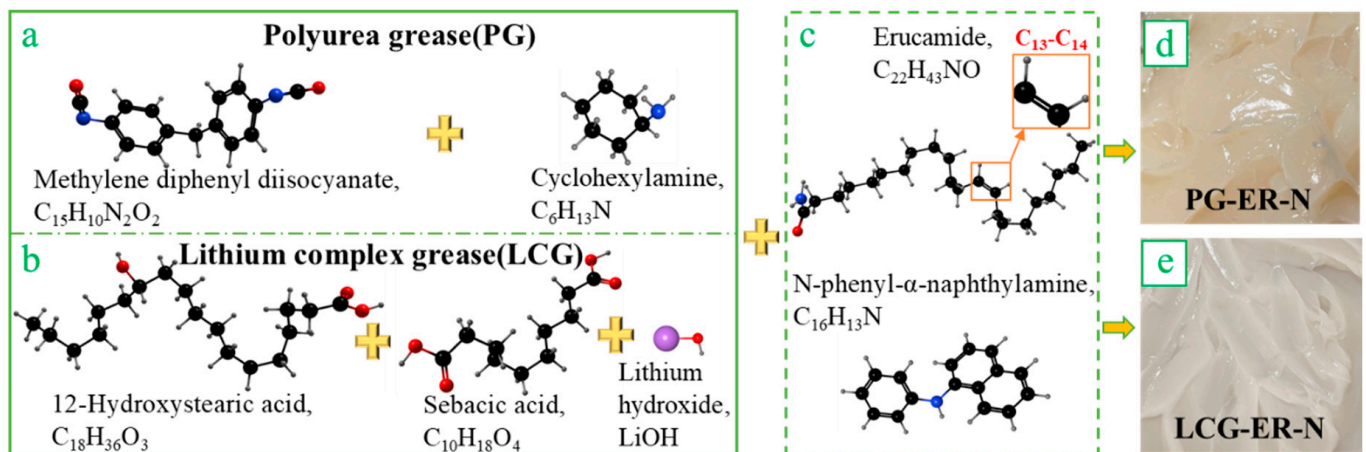


Figure 1. Chemical reactions in the preparation of greases. ((a) Formation of polyurea thickener; (b) Formation of lithium complex thickener; (c) Add erucamide and N-phenyl- α -naphthylamine; (d) PG-ER-N grease; (e) LCG-ER-N grease.)

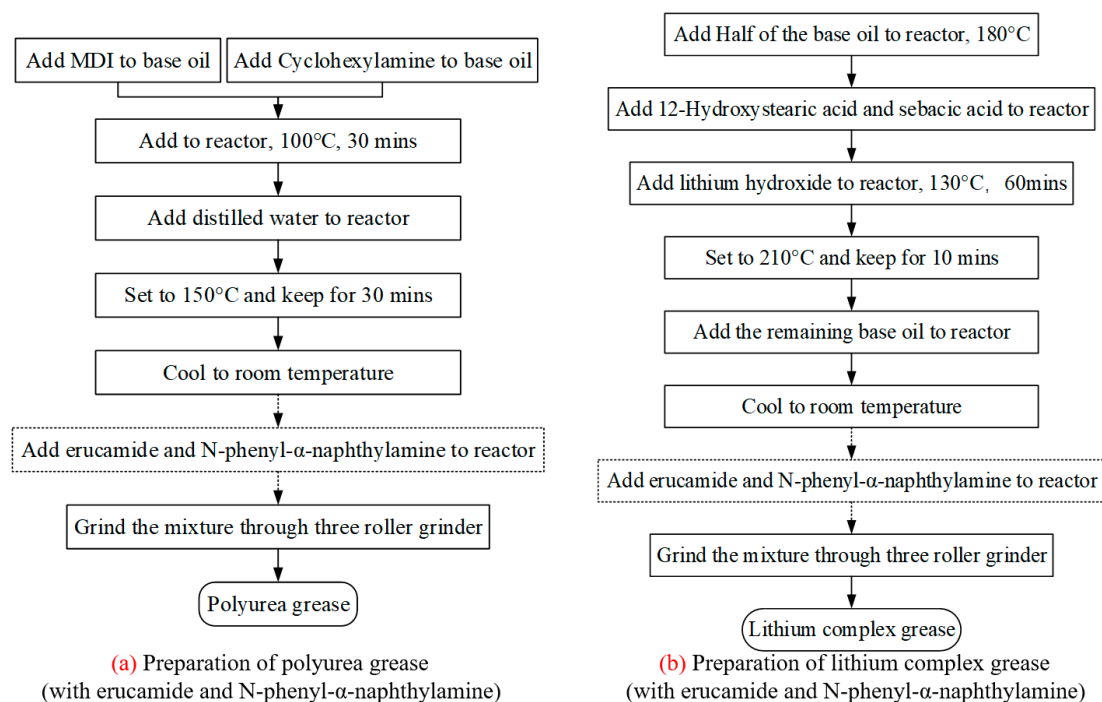


Figure 2. Flow chart of grease preparation.

2.2.2. Preparation of Lithium Complex Grease

Lithium complex grease was prepared through a high-temperature blending process of 12-Hydroxystearic acid, sebacic acid, and lithium hydroxide in a base oil, as illustrated in Figure 1b. In this formulation, the LCG thickener was derived from the saponification reaction of 12-Hydroxystearic acid, sebacic acid, and lithium hydroxide. A flow chart of the lithium complex grease preparation process is shown in Figure 2b. The specific preparation procedure was divided into five steps:

- Half of the base oil was introduced into the reactor and heated to 80 °C.
- 12-Hydroxystearic acid and sebacic acid were added to the reactor and continuously stirred until fully dissolved.
- A solution of lithium hydroxide was poured into the reactor, with continuous stirring. The temperature of the reactor was set to 130 °C and maintained for 60 min.
- The temperature of the reactor was raised to 210 °C and held for 10 min.
- The remaining half of the base oil was added to the reactor, and the reactor's temperature was lowered to room temperature.
- The mixture was poured into a three-roller grinder for grinding to obtain LCG.

2.2.3. Preparation of Grease with Erucamide and N-phenyl- α -naphthylamine

Erucamide, with a purity exceeding 98%, was supplied by USOLF Corporation, while N-phenyl- α -naphthylamine, also with a purity exceeding 98%, was provided by the MACKLIN Corporation. Erucamide and N-phenyl- α -naphthylamine (as depicted in Figure 1c) were added into the two grease formulations mentioned earlier, serving as the experimental group (as shown in Figure 1d), whereas the two original greases constituted the control group.

The specific preparation process for the experimental group grease was as follows: After the reactor temperature cooled to room temperature (Step d in Section 2.2.1 and Step e in Section 2.2.2), erucamide and N-phenyl- α -naphthylamine were separately added into the reactor and stirred for 30 min to ensure even distribution (dotted box in Figure 2). Finally, the mixture was poured into a three-roller grinder for grinding to obtain the experimental group grease, as shown in Figure 1d,e. The composition and mass fractions of greases are detailed in Table 2. For ease of reference, the grease samples are denoted as PG-ER-N (e,n) or LCG-ER-N (e,n), where PG represents polyurea grease, LCG represents lithium

complex grease, ER represents erucamide, N represents N-phenyl- α -naphthylamine, e represents the mass fraction of erucamide, and n represents the mass fraction of N-phenyl- α -naphthylamine. In addition, the grease itself was of low toxicity. If not handled properly, it will cause environmental pollution and damage, so it was necessary to strengthen the management and maintenance of grease.

Table 2. The composition and mass fractions of greases.

Number	Grease Samples	Base Oil, wt. %	Thickener, wt. %	ER, wt. %	N, wt. %
1	PG-ER-N (0,0)	PAO4, 80		0	0
2	PG-ER-N (0,3)	PAO4, 77		0	3
3	PG-ER-N (1,2)	PAO4, 77	polyurea, 20	1	2
4	PG-ER-N (2,1)	PAO4, 77		2	1
5	PG-ER-N (3,0)	PAO4, 77		3	0
6	LCG-ER-N (0,0)	PAO4, 80		0	0
7	LCG-ER-N (0,3)	PAO4, 77		0	3
8	LCG-ER-N (1,2)	PAO4, 77	lithium, 20	1	2
9	LCG-ER-N (2,1)	PAO4, 77		2	1
10	LCG-ER-N (3,0)	PAO4, 77		3	0

2.2.4. Structure Characterization of Thickener

To observe the structural characteristics of thickener, it was necessary to separate the base oil and thickener in the grease. This process was divided into 8 steps:

- a. A small quantity of grease was poured into petroleum ether, thoroughly dissolved, and then the mixture was poured into a centrifuge tube.
- b. The centrifuge tube was placed in a centrifuge machine (JOANLAB MC-7K), centrifuged at a rotational speed of 7000 rpm for 30 min at room temperature, followed by 30 min of static settling.
- c. Step 2 was repeated three times.
- d. The upper clear liquid in the centrifuge tube was poured out, leaving behind the precipitate.
- e. Petroleum ether was added again to the centrifuge tube and allowed to settle for 30 min, ensuring thorough dissolution of the precipitate in petroleum ether.
- f. Steps 2–5 were repeated twice, and then Steps 2–4 were repeated once.
- g. The final precipitate was placed on a silicon wafer for drying.
- h. In a vacuum environment, an ion sputtering instrument (HITACHI E-1045) was used for gold sputtering treatment of the silicon wafer, with a sputtering time of 100 s and three sputtering cycles.

Finally, the thickener's structure was observed by scanning electron microscopy (SEM, Zeiss Ultra Plus, Jena, Germany).

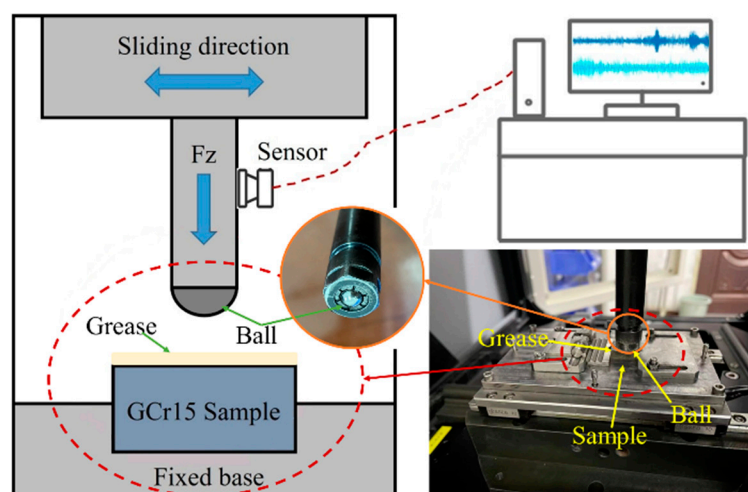
2.3. Tribological Test

The friction pair samples comprised GCr15 steel blocks and Si₃N₄ steel balls. The main constituents of the GCr15 steel are detailed in Table 3, with geometric dimensions of 16 mm × 12 mm × 6 mm, and the Si₃N₄ steel balls had a diameter of 6.3 mm. The surfaces of the GCr15 steel were sequentially polished using 1200# and 2000# sandpaper on a metallographic polishing machine (MP-1B) with a rotational speed of 1000 rpm and a polishing duration of 30 min. The profile parameters of the sample surfaces were measured using a 3D optical profilometer (UP-3D, Rtec) at ten random locations on each sample to ensure that the surface roughness of all samples was less than 0.05 μ m. Finally, all samples were subjected to ultrasonic cleaning in alcohol for 10 min.

Table 3. The main constituents of the GCr15 steel.

Element	C	Cr	Mn	Si	P	S	Fe
Wt. %	0.95–1.05	1.4–1.65	0.2–0.4	0.15–0.35	≤0.027	≤0.02	2.747–3.497

To investigate the tribological properties of greases with different formulations on the GCr15 steel, the MFT-5000 friction tester test system was established, as shown in Figure 3. During the testing process, friction coefficients were recorded. GCr15 steel blocks and Si₃N₄ steel balls were securely affixed to fixtures. A uniform application of 3 mm of grease was made on the surface of the steel blocks. The testing method involved reciprocating friction, with the testing conditions detailed in Table 4. Real-time variations in frictional force and load were collected by a sensor on the MFT-5000 reciprocating friction testing machine (Rtec Instruments, SAN Jose, Silicon Valley, CA, USA), with a data sampling frequency of 100 values per second. Six thousand friction coefficients were collected per minute. The test results for the friction coefficients were calculated by averaging the data in 1 s intervals, and each test was repeated three times.

**Figure 3.** Schematic diagram and photos of MFT-5000 reciprocating friction testing machine.**Table 4.** The testing conditions.

Reciprocating Distance/mm	Reciprocating Frequency/Hz	Test Load (Fz)/N	Test Time/min
8	1	20	30

2.4. Friction Torque Test

Deep-groove ball bearings (6206 2RS1/C3) were selected for the study, supplied by SKF Limited, with an inner diameter of 30 mm, an outer diameter of 62 mm, and a width of 16 mm. A total of 11 sets of bearings were prepared. One set of bearings was kept without the addition of grease for the control group, while the remaining ten sets of bearings were each lubricated with 6 g of grease. The type of grease added in each set was determined according to the grease samples, as shown in Table 2.

The friction torque of the deep-groove ball bearings with ten different types of grease and those without grease was tested using the M9915 bearing friction torque testing machine, as shown in Figure 4. To address the issue of uneven grease distribution within the bearings, a pre-treatment of the bearings was conducted. The bearings were mounted on the M9915 bearing friction torque testing machine, with the fixture securing the outer ring of the bearing. The drive component was fixed to the inner ring, and a 100 N axial load was applied to the bearing through the drive component. The bearing's inner ring

was rotated by the drive component at a clockwise rotation speed of 900 rpm for 30 min. Afterward, the bearings were left undisturbed for a minimum of 12 h, allowing them to cool to room temperature before testing them.

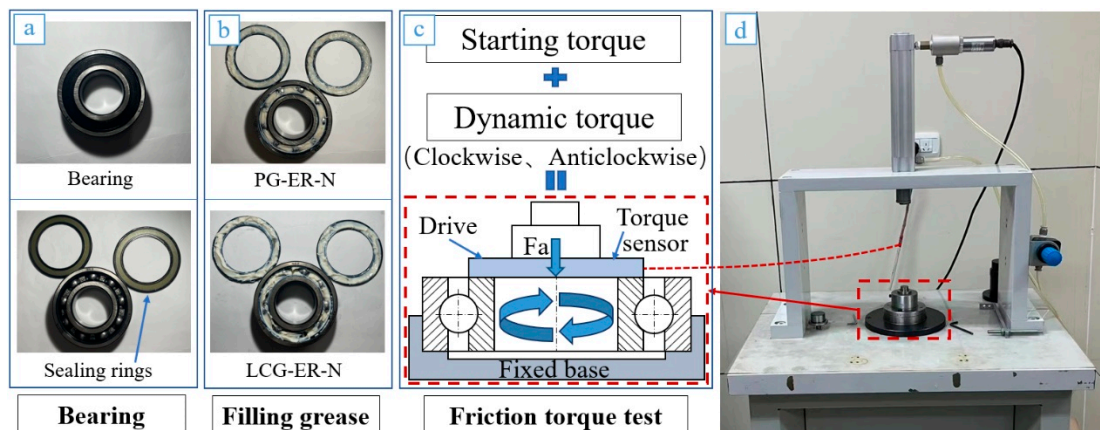


Figure 4. Friction torque test. (a) Bearing physical drawing; (b) Add grease to bearing; (c) Friction torque test principle; (d) Friction torque testing machine.).

The tests were conducted following the standard GB/T 32562-2016 “Rolling bearings—Measuring methods for friction torque” [36]. A torque sensor was mounted on the drive component to automatically collect friction torque data. As the drive component progressively increased the rotational speed of the bearing’s inner ring, the inner ring rotated clockwise 180° (half a turn) relative to the fixed outer ring. Throughout this process, the maximum torque value recorded by the torque sensor was identified as the starting torque. Subsequently, the bearing’s inner ring was rotated at a rotational speed of 100 rpm, both clockwise and counterclockwise, for 30 min each, and the torque sensor measured the friction torque, which was considered as the dynamic torque. Each test was repeated three times.

2.5. Surface Analysis and Characterization

Following the friction tests, the 3D wear scars on the surface of the GCr15 steel samples were measured using a 3D optical profilometer (UP-3D Rtec). The morphology of the worn surfaces was captured using an electron probe microanalyzer (JAXA-8230) (EPMA) to analyze the microstructural features of the sample’s worn surface. Elemental analysis of the worn scars on the surface was performed using an X-ray energy-dispersive spectrometer (INCA-X-ACT) (EDS) to observe the distribution characteristics of elements on the worn surface. This analysis allowed for the investigation of friction chemical reactions on the worn surface and the assessment of wear damage.

3. Results and Discussion

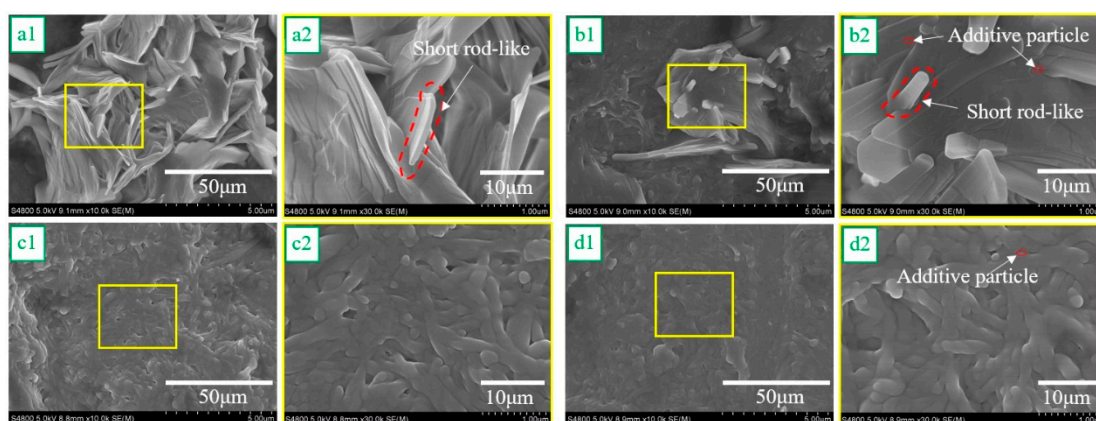
3.1. Physicochemical Properties of Greases

The physicochemical properties of the two greases were tested. As shown in Table 5, the work cone penetration and extended work cone penetration are indicators of the grease’s consistency and hardness. Larger values denote lower consistency, meaning that the PG is softer and exhibits greater flowability. The difference between the extended work cone penetration and work cone penetration, known as shear stability, reflects the ability of the grease to maintain its structural integrity. A smaller difference indicates better shear stability. Oil separation is utilized to assess the base oil’s ability to seep out from the thickener. PG exhibits a higher degree of oil separation, signifying a greater propensity for base oil to separate from the thickener.

Table 5. Physicochemical properties of greases.

Test Projects	PG-ER-N (0,0)	LCG-ER-N (0,0)	Test Method
Worked cone penetration (0.1 mm)	289	272	GB/T 269
Extended worked cone penetration (10,000 times, 0.1 mm)	303	296	GB/T 269
The difference between the extended work cone penetration and work cone penetration	24	26	/
Oil separation (100 °C, 24 h) % (m/m)	2.31	1.79	NB/SH/T 0324

To further investigate the influence of erucamide, N-phenyl- α -naphthylamine, and thickener on grease performance, low- and high-magnification scanning electron microscopy (SEM) images of the four degreased greases are presented in Figure 5. As shown in Figure 5(a1,a2,b1,b2), the polyurea thickener consisted of short rod-like fibers that closely aggregate to form a large-area lamellar structure. Additive particles and base oil were trapped between the lamellar structures. Figure 5(c1,c2,d1,d2) reveal that the lithium complex thickener was composed of fibers with varying lengths and thicknesses, which coiled together in a spiral fashion, forming a network structure capable of effectively entrapping the base oil, with additives dispersed between the fiber structures. These physicochemical characteristics are reflected in the low values of worked cone penetration and oil separation.

**Figure 5.** Low- and high-magnification scanning electron microscopy (SEM) images of the four degreased greases.

3.2. Friction and Wear Effects of Greases

Each test was repeated three times, and the average friction coefficient per second was used as the test result, as shown in Figure 6(A1,B1). The friction coefficient curve indicated a rapid initial increase followed by gradual stabilization, with the PG-ER-N series achieving a shorter time to reach stability and greater overall stability. As depicted in Figure 6(A2,B2), the average friction coefficient of PG-ER-N (0,3) was 0.0026 less than that of PG-ER-N (0,0), while the average friction coefficient of LCG-ER-N (0,3) was 0.0406 less than that of LCG-ER-N (0,0), suggesting that adding N-phenyl- α -naphthylamine to the PG or LCG has minimal friction-reducing effects. PG-ER-N (3,0) exhibited a 0.0431 lower average friction coefficient than PG-ER-N (0,0), and LCG-ER-N (3,0) displayed a 0.0406 lower average friction coefficient than LCG-ER-N (0,0), indicating the significant friction-reducing effect of the erucamide added to the PG or LCG. The ranking of the average friction coefficient in PG and LCG remains consistent, with the best friction-reducing effect observed for ER-N (2,1). The cooperative tribological performance of erucamide, N-phenyl- α -naphthylamine, and PG was superior.

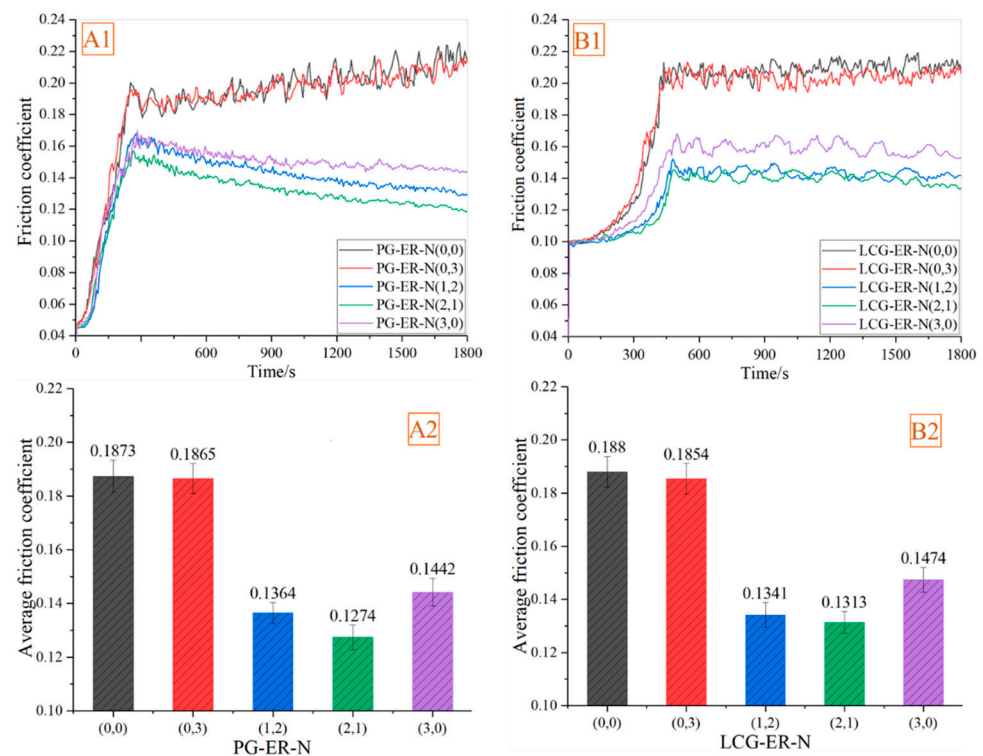


Figure 6. Friction coefficient curves and average friction coefficient of different greases. ((A1) Friction coefficient curve of PG; (B1) Friction coefficient curve of LCG; (A2) Average friction coefficient curve of PG; (B2) Average friction coefficient curve of LCG.).

The instantaneous friction coefficient curve for the 900~903 s period of PG is illustrated in Figure 7. During the reciprocating friction in a stable state, the friction coefficient curve exhibits a wavering pattern. This phenomenon is attributed to the lamellar thickener and the adsorbed base oil, which formed an oil film between the friction pair, serving as a barrier and reducing the friction coefficient. As the reciprocating friction continued, the thickener and base oil were compressed and moved outward, disrupting the oil film and leading to an increase in the friction coefficient.

The friction coefficient curve for the 900~903 s period of LCG is depicted in Figure 8. In the stable state, the curve exhibits periodic fluctuations, initially decreasing sharply, followed by gradual minor oscillations, and finally a rapid increase. This phenomenon can be attributed to the separation of base oil within the network thickener, which formed an oil film between the friction pair, preventing direct contact and thereby reducing the friction coefficient. As the friction test continued with reciprocating motion, under the influence of shear forces, the grease was continuously sheared, and the network thickener was continuously disrupted, consequently destroying the oil film. This led to an increase in the friction coefficient and a rise in the contact area's temperature. The elevated temperature resulted in a reduction in the viscosity of the base oil in the contact area, increasing its flowability. The enhanced fluidity of the base oil brought new grease into the contact area, forming a fresh oil film. This process repeated itself as the fibrous thickener was repeatedly sheared, causing alternating decreases and increases in the friction coefficient.

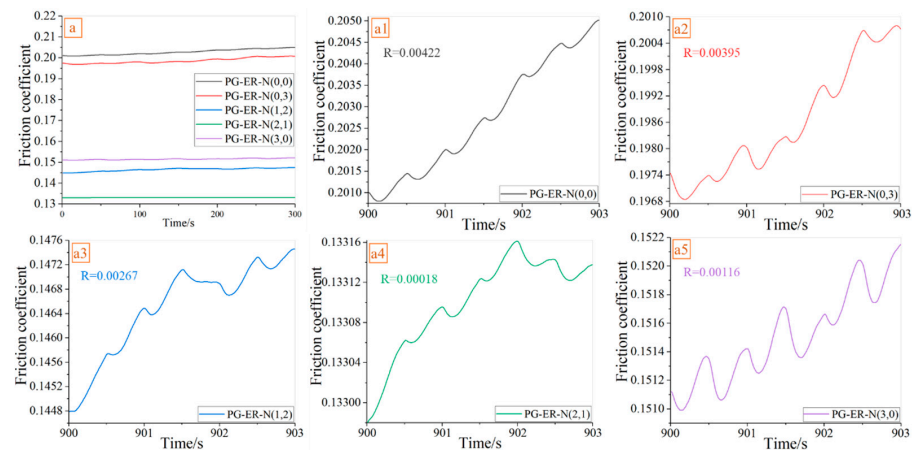


Figure 7. The friction coefficient curve of all PG at 900~903 s. ((a) The friction coefficient curve of PG at 900~903 s; (a1) The friction coefficient curve of PG-ER-N(0,0) at 900~903 s; (a2) The friction coefficient curve of PG-ER-N(0,3) at 900~903 s; (a3) The friction coefficient curve of PG-ER-N(1,2) at 900~903 s; (a4) The friction coefficient curve of PG-ER-N(2,1) at 900~903 s; (a5) The friction coefficient curve of PG-ER-N(3,0) at 900~903 s.).

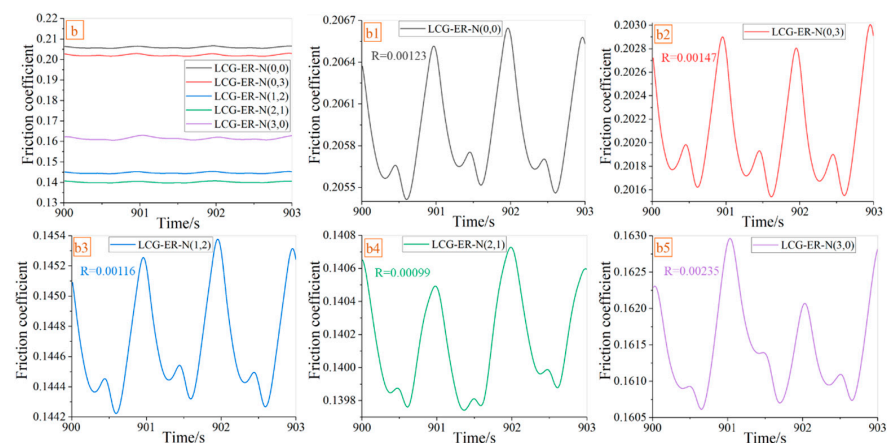


Figure 8. The friction coefficient curve of all LCG at 900~903 s. ((b) The friction coefficient curve of LCG at 900~903 s; (b1) The friction coefficient curve of LCG-ER-N(0,0) at 900~903 s; (b2) The friction coefficient curve of LCG-ER-N(0,3) at 900~903 s; (b3) The friction coefficient curve of LCG-ER-N(1,2) at 900~903 s; (b4) The friction coefficient curve of LCG-ER-N(2,1) at 900~903 s; (b5) The friction coefficient curve of LCG-ER-N(3,0) at 900~903 s.).

Combining the information from Figures 7 and 8, it can be observed that PG-ER-N (2,1) (Figure 7(a4)) and LCG-ER-N (2,1) (Figure 8(b4)) had the smallest range (R), which represents the difference between the maximum and minimum values of the friction coefficient curve. This indicates minimal fluctuations in the friction coefficient. PG-ER-N (3,0) (Figure 7(a5)) and LCG-ER-N (3,0) (Figure 8(b5)) had the second-smallest range, with slightly larger range values. In contrast, PG-ER-N (0,0), PG-ER-N (0,3), LCG-ER-N (0,0), and LCG-ER-N (0,3) all exhibited larger range values, indicating that the addition of erucamide in PG or LCG has a favorable antifriction effect. The addition of N-phenyl- α -naphthylamine led to a slight reduction in friction, while ER-N (2,1) provided the best antifriction effect. This macroscopic behavior is consistent with what can be observed in Figure 6.

As shown in Figure 9, both PG-ER-N (0,0) and PG-ER-N (0,3) exhibited numerous deep spalling pits, along with minor wear debris and furrows. Combined with Figure 9(a2,b2,f1,f2), it is apparent that the samples' surfaces suffered severe oxidative wear. Upon a further inspection, as shown in Figure 9(a3,b3), an increase in Si (as indicated in Table 3, where the Si element content is 0.15~3.5%) and a decrease in Fe elements on the sample's surface were observed. This is attributed to the breakdown of the oil film formed by the base oil, which

failed to provide a protective isolation effect. Consequently, direct contact between the friction pair resulted in the formation of an adhesion effect, leading to shear fractures on the contact surface and in deeper layers of the samples. This process resulted in severe wear. In the friction pair, Si elements from the Si_3N_4 ball migrated to the GCr15 steel surface. This contributed to adhesive wear, coupled with the formation of an oxide film. Hence, it can be deduced that adding only N-phenyl- α -naphthylamine to PG does not yield a noticeable antifriction effect.

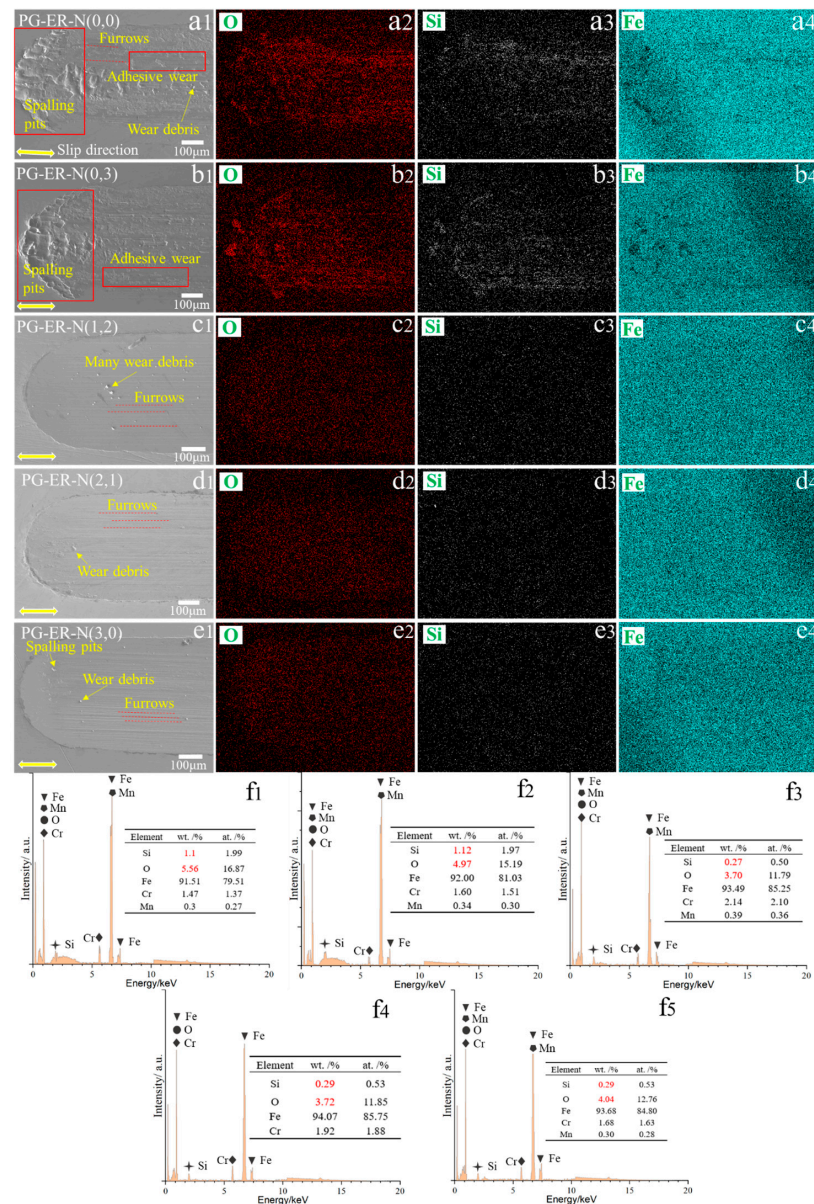


Figure 9. EPMA and EDS images of wear of PG sample's surface. ((a1) EPMA images of wear of PG-ER-N(0,0) sample's surface; (a2–a4) EDS images of PG-ER-N(0,0) sample's surface; (b1) EPMA images of wear of PG-ER-N(0,3) sample's surface; (b2–b4) EDS images of PG-ER-N(0,3) sample's surface; (c1) EDS images of wear of PG-ER-N(1,2) sample's surface; (c2–c4) EDS images of PG-ER-N(1,2) sample's surface; (d1) EPMA images of wear of PG-ER-N(2,1) sample's surface; (d2–d4) EDS images of PG-ER-N(2,1) sample's surface; (e1) EPMA images of wear of PG-ER-N(3,0) sample's surface; (e2–e4) EDS images of PG-ER-N(3,0) sample's surface; (f1) Elemental content of PG-ER-N(0,0); (f2) Elemental content of PG-ER-N(0,3); (f3) Elemental content of PG-ER-N(1,2); (f4) Elemental content of PG-ER-N(2,1); (f5) Elemental content of PG-ER-N(3,0).).

The surfaces of PG-ER-N (1,2), PG-ER-N (2,1), and PG-ER-N (0,3) exhibited wear debris and furrows of varying depths. The samples' surfaces underwent abrasive wear, along with minor oxidative wear, as indicated in Figure 9(c2,d2,e2,f3–f5). Therefore, the addition of erucamide to PG has a significant antifriction effect. This effect is due to the formation of an oil film between the friction pairs, where the erucamide molecules attached to the lamellar polyurea thickener transform sliding friction into rolling friction. Consequently, the tribological properties of PG were notably improved.

As shown in Figure 10, the surfaces of both LCG-ER-N (0,0) and LCG-ER-N (0,3) exhibited numerous deep spalling pits and peeling. In conjunction with Figure 10(a2–a4,b2–b4,f1,f2), it is evident that the sample surfaces suffered severe oxidative wear and adhesive wear. This was due to the insufficient formation of an oil film to protect the samples from breakdown, as the base oil that separates from the fibrous lithium complex thickener did not provide enough of a film. It can be inferred that the addition of N-phenyl- α -naphthylamine alone to LCG does not yield any noticeable antifriction effects.

The surfaces of LCG-ER-N (1,2), LCG-ER-N (2,1), and LCG-ER-N (0,3) exhibited only minor wear debris, shallow furrows, and small peeling pits. The sample surfaces exhibited abrasive wear, accompanied by oxidative wear, as shown in Figure 10(c2,d2,e2,f3–f5). Therefore, it is clear that the addition of erucamide to LCG results in a significant reduction in friction. This is due to the progressive development of an oil film formed by the base oil exuding from the fibrous thickener during reciprocating friction. In the process of oil film thickness reduction, erucamide molecules play a role in isolation, transforming sliding friction into rolling friction. As a result, the tribological properties of LCG were noticeably improved.

The 3D surface mapping and 2D profiles of the worn surfaces of PG samples are presented in Figure 11, while the corresponding data for LCG samples are shown in Figure 12. Notably, the wear scars on the PG samples exhibited greater depth, whereas the wear scars on the LCG samples were wider. A comparison between Figures 11 and 12 reveals that the wear scars on the LCG samples were rougher, indicating more severe wear.

As shown in Figure 13, the surface roughness (R_a) of PG and LCG exhibited the same ranking in ascending order: (0,0), (0,3), (3,0), (1,2), and (2,1). This ranking corresponds to the order of the average friction coefficients, as shown in Figure 6. In comparison to ER-N (0,0), ER-N (0,3) exhibited a slight reduction in surface roughness. This can be attributed to the formation of an oil film primarily by the base oil during the friction process, which served an insulating protective function. Meanwhile, N-phenyl- α -naphthylamine, as an antioxidant, reduced the oxidative degradation of the base oil. Consequently, the base oil can offer better protection to the sample surface. As a result, N-phenyl- α -naphthylamine indirectly contributed to the reduction in friction. Therefore, the addition of N-phenyl- α -naphthylamine to the PG or LCG has a mild friction-reducing effect.

In contrast to ER-N (0,0), ER-N (3,0) demonstrated a significant reduction in surface roughness, affirming the excellent tribological properties achieved by adding erucamide to the PG or LCG. ER-N (2,1) exhibited the lowest surface roughness, with the surface roughness of PG-ER-N (2,1) being as low as 0.07, underscoring the superior antifriction effect of ER-N (2,1). Compared to LCG, it showed an enhanced synergistic antifriction performance with PG.

When $R_{ku} > 3$ and continued to increase, the peaks on the sample surface became clearer and sharper [37]. Such sharp peaks can lead to stress concentration and exacerbate surface wear. As shown in Figure 13b, LCG-ER-N (0,0) exhibited the highest R_{ku} value, which was 10.382, resulting in pronounced and sharp surface peaks. This led to severe wear on the sample surface (corresponding to Figure 10(a1)). In contrast, PG exhibited the lowest R_{ku} value of 6.604, which translated into less prominent surface peaks and resulted in mild wear on the sample surface (corresponding to Figure 9(a1)).

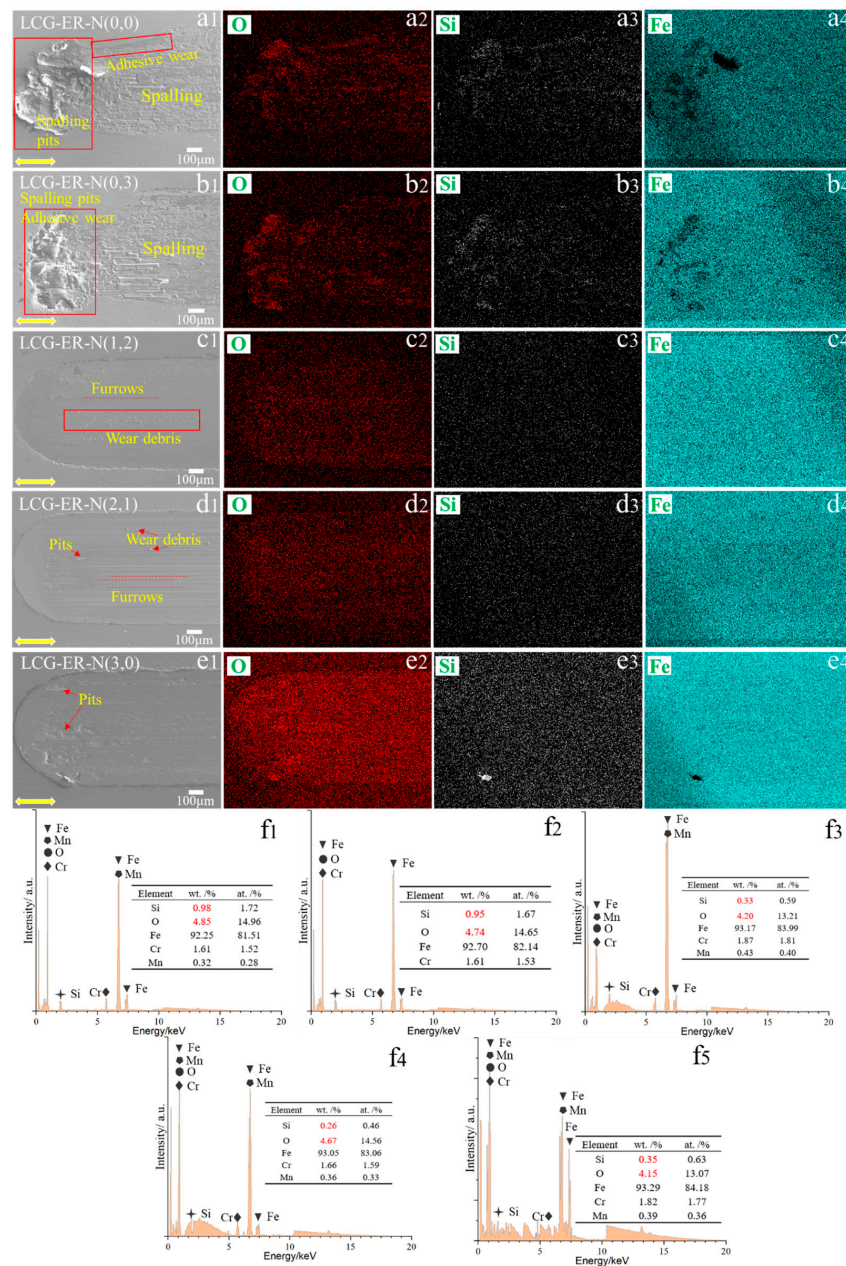


Figure 10. EPMA and EDS images of wear of LCG sample's surface. ((a1) EPMA images of wear of LCG-ER-N(0,0) sample's surface; (a2–a4) EDS images of LCG-ER-N(0,0) sample's surface; (b1) EPMA images of wear of LCG-ER-N(0,3) sample's surface; (b2–b4) EDS images of LCG-ER-N(0,3) sample's surface; (c1) EPMA images of wear of LCG-ER-N(1,2) sample's surface; (c2–c4) EDS images of LCG-ER-N(1,2) sample's surface; (d1) EPMA images of wear of LCG-ER-N(2,1) sample's surface; (d2–d4) EDS images of LCG-ER-N(2,1) sample's surface; (e1) EPMA images of wear of LCG-ER-N(3,0) sample's surface; (e2–e4) EDS images of LCG-ER-N(3,0) sample's surface; (f1) Elemental content of LCG-ER-N(0,0); (f2) Elemental content of LCG-ER-N(0,3); (f3) Elemental content of LCG-ER-N(1,2); (f4) Elemental content of LCG-ER-N(2,1); (f5) Elemental content of LCG-ER-N(3,0).).

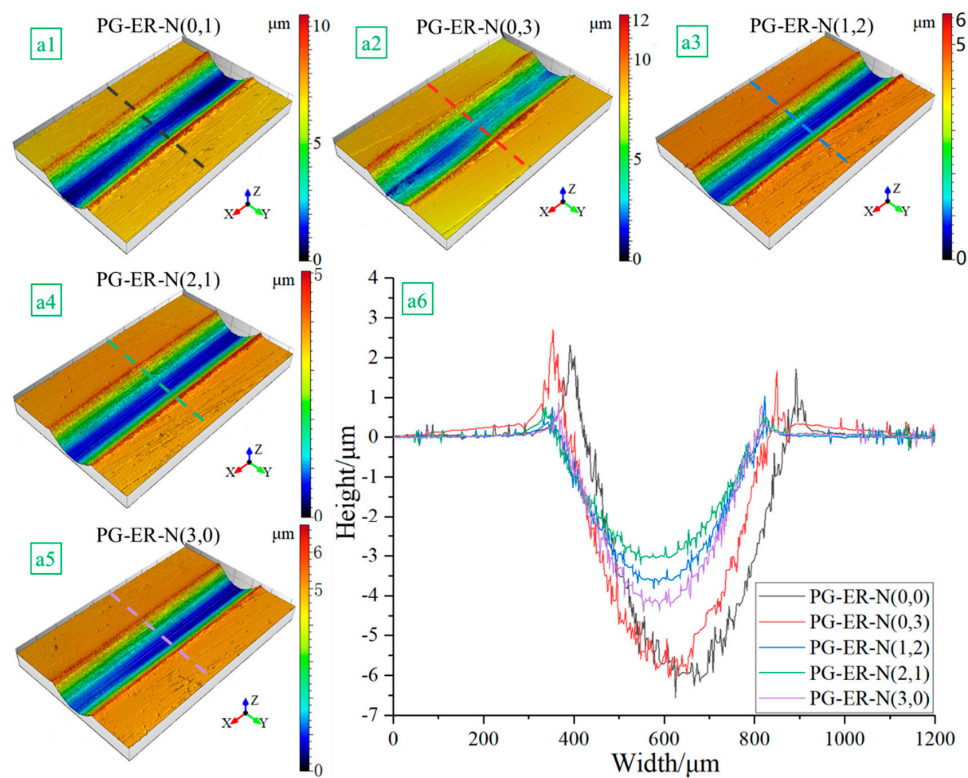


Figure 11. 3D surface mapping (a1–a5) and 2D profile (a6) of PG sample wear.

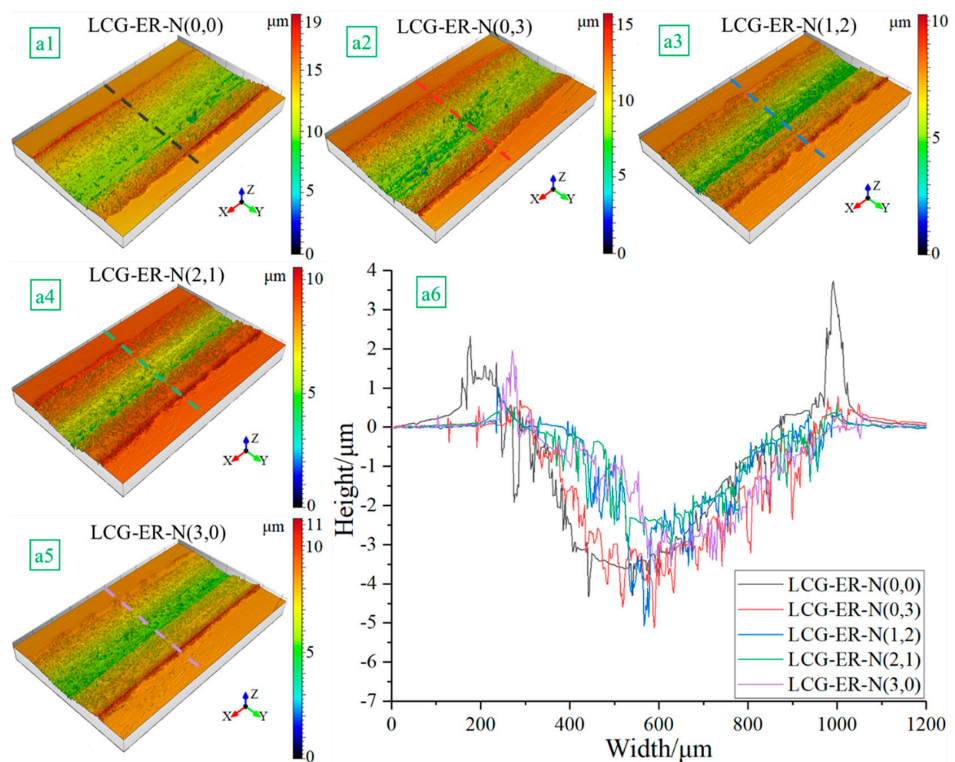


Figure 12. 3D surface mapping (a1–a5) and 2D profile (a6) of LCG sample wear.

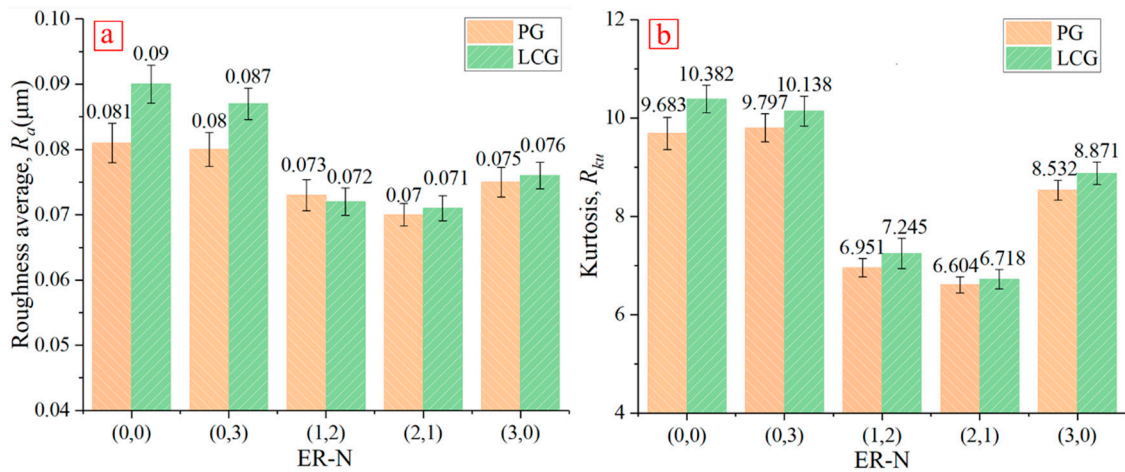


Figure 13. Changes in profile parameters of the worn surfaces. ((a) Surface roughness of PG and LCG; (b) Kurtosis of PG and LCG).

3.3. Lubrication Mechanism Analysis

The reciprocating friction test model is depicted in Figure 14a. The erucamide model is illustrated in Figure 14b. At low concentrations, the arrangement of erucamide molecules formed a monolayer structure. With increasing concentration, the arrangement of erucamide molecules transitioned into bilayer or even multilayer structures.

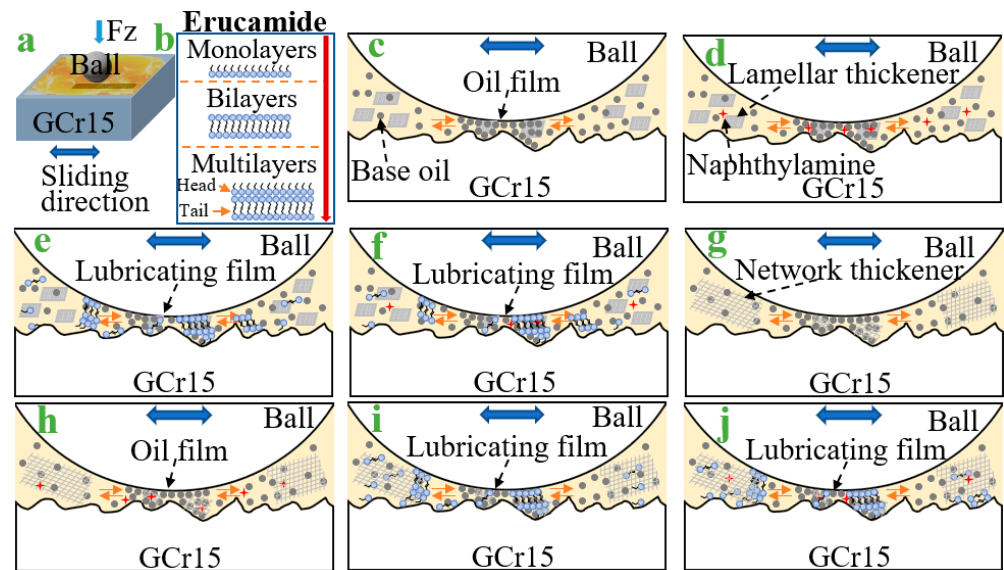


Figure 14. Lubrication mechanism analysis. ((a) Friction model; (b) Molecular structure of erucamide; (c–f) Lubrication mechanism of PG; (g–j) Lubrication mechanism of LCG).

As shown in Figure 14c, the lubrication model for PG-ER-N (0,0) featured a lamellar thickener composed of short rods of varying lengths, with the base oil positioned between the thickener layers. During the reciprocating sliding of the Si_3N_4 ball, the base oil formed an oil film between the friction pair, and the lamellar thickener acted in conjunction with this oil film to provide lubrication and isolation for sample surfaces, thereby achieving a friction reduction effect.

As illustrated in Figure 14d, the lubrication model for PG-ER-N (0,3) shared a similar friction reduction mechanism with PG-ER-N (0,0), where the base oil's formation of an oil film played a key role in reducing friction. However, the key difference is that PG-ER-N (0,3) contained an addition of N-phenyl- α -naphthylamine, which acts as an antioxidant.

This antioxidant effect helped slow down the oxidation of the base oil, extending the oil's lifespan, which indirectly contributed to friction reduction.

Figure 14e illustrates the lubrication model for PG-ER-N (3,0), and its lubrication mechanism builds upon that of PG-ER-N (0,0) by incorporating erucamide. Erucamide compensates for any gaps left when the oil film or lamina thickener are disrupted. Additionally, erucamide molecules form tighter bonds through pi-pi stacking interactions generated by the double bond between C₁₃-C₁₄ [24] (in Figure 1c). These interactions help maintain a more cohesive bond, and erucamide molecules, along with the oil film, collectively form a lubricating film. Furthermore, erucamide converts the sliding friction of the lamina thickener into rolling friction. This transformation provides better protection to the friction pair surfaces, preventing damage more effectively than a sole oil film. As shown in Figure 14f, the lubrication model for PG-ER-N (2,1) and PG-ER-N (1,2) combines the lubrication mechanisms of both PG-ER-N (0,3) and PG-ER-N (3,0).

As depicted in Figure 14g, the lubrication model for LCG-ER-N (0,0) exhibits a network thickener made up of interwoven fibers, enveloping the base oil. During reciprocating frictional motion, the network thickener is compressed, resulting in the release of base oil that is subsequently absorbed. When released, the base oil forms an oil film, protecting the friction pair surfaces and reducing friction. However, during absorption, the base oil content in the oil film decreases, causing the film to thin and, in turn, increasing friction. This phenomenon leads to the periodic variation in friction coefficients, as observed in Figure 8.

As shown in Figure 14h, the lubrication model for LCG-ER-N (0,3) follows the same lubrication mechanism as LCG-ER-N (0,0). Additionally, the presence of N-phenyl- α -naphthylamine in the grease, acting as an antioxidant, indirectly contributes to friction reduction.

The model for LCG-ER-N (3,0), displayed in Figure 14i, builds upon the base lubrication mechanism of LCG-ER-N (0,0). In cases where the base oil is either absorbed or disrupted, erucamide promptly fills the voids, forming a lubricating film in conjunction with the base oil. This combined effect provides enhanced protection for the friction pair, preventing damage more effectively. In Figure 14j, the lubrication models for LCG-ER-N (2,1) and LCG-ER-N (1,2) combine the friction reduction mechanisms of both LCG-ER-N (0,3) and LCG-ER-N (3,0).

3.4. Verifying Friction Torque Test Results

The magnitude of the starting torque and dynamic torque of bearings has a significant impact on the stability and reliability of the entire vehicle transmission system. The starting torque represents the maximum frictional torque required for the bearing to transition from a stationary state to rotation. This phase is crucial in the wear of roller bearings. During the startup process, a complete oil film is not formed between the rolling elements and the inner and outer rings of deep-groove ball bearings. Lubrication is primarily dependent on thickeners and additives. As illustrated in Figure 15a, the starting torque was smallest for the NO.G (no grease). This is because, during the startup, the bearing not only needs to overcome its own resistance but also has to overcome the resistance of the grease, which must be set into motion along with the bearing. In the NO.G, where no grease is present, the absence of grease resistance resulted in the smallest starting torque.

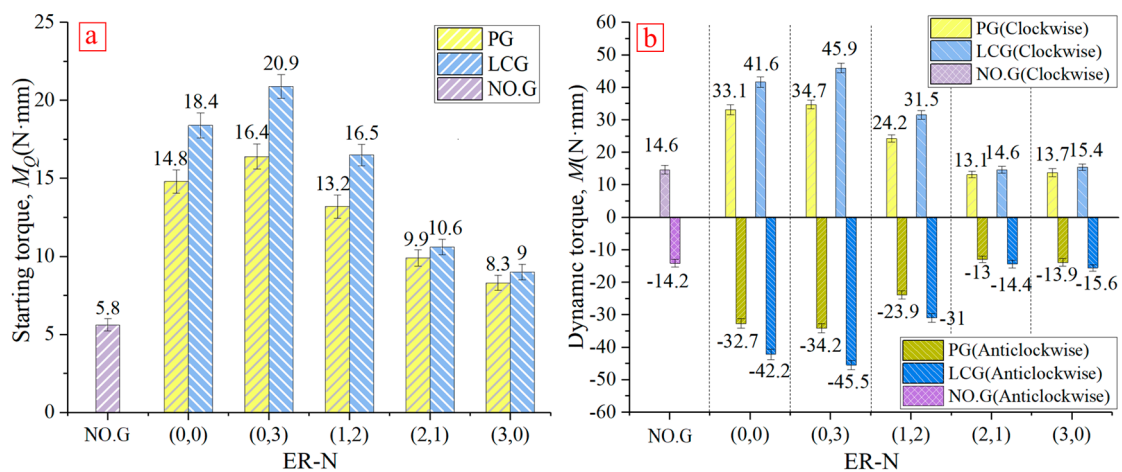


Figure 15. Starting torque (a) and dynamic torque (b) of deep-groove ball bearing.

For ER-N (0,0), the starting torque of PG was smaller than that of LCG. This can be attributed to the lower consistency of PG, which makes it softer, and the lamellar thickeners that help to separate the rolling elements from the inner and outer rings. The starting torque of ER-N (0,3) was higher than that of ER-N (0,0). This is because, within an extremely short period at startup, N-phenyl- α -naphthylamine molecules distributed among the grease add to the grease's resistance, causing a friction-increasing effect.

ER-N (3,0) exhibited the smallest starting torque, indicating a notable friction reduction effect of erucamide. This can be attributed to the unique structure of erucamide, acting as a barrier between the rolling elements and the inner and outer rings. This transformation reduces sliding friction into rolling friction, significantly decreasing resistance. PG-ER-N (3,0) exhibited the smallest starting torque [38], demonstrating an enhanced cooperation between erucamide and PG.

The performance of bearings during stable rotation plays a decisive role in their lifespan. Clockwise and counterclockwise rotations mutually corroborate, providing a better simulation of real operating conditions for bearings. As shown in Figure 15b, the dynamic torque, as compared to the starting torque, increased the friction torque by 151.72% $((14.6-5.8)/5.8)$ for NO.G, 123.65% for PG-ER-N (0,0), and 129.35% for LCG-ER-N (0,0). This suggests that bearings without grease experience a sharp increase in friction torque. It can be predicted that over time, bearings without grease will deteriorate more quickly than those with grease. Therefore, the addition of grease to bearings is of paramount importance for increasing their lifespan and stability.

The friction torque for PG-ER-N (0,3) and LCG-ER-N (0,3) increased by 111.59% and 119.62%, respectively. In comparison to PG-ER-N (0,0) and LCG-ER-N (0,0), the rate of increase in friction torque was slightly reduced. This was due to the addition of N-phenyl- α -naphthylamine in PG and LCG, which acts as an antioxidant, retarding the oxidation of the base oil and prolonging its lubrication effectiveness. The frictional torques of PG ER-N (3,0) and LCG ER-N (3,0) increased by 67.47% and 73.33%, respectively. This increase in frictional torque, when compared to PG-ER-N (0,0) and LCG-ER-N (0,0), exhibited a significantly reduced growth rate. This reduction can be attributed to the effective friction-reducing properties of erucamide within the grease during stable rotation. The friction torque increased by 32.32% for PG-ER-N (2,1) and 37.74% for LCG-ER-N (2,1), with the smallest rate of increase in friction torque. The dynamic torque was also the smallest, particularly for PG-ER-N (2,1). ER-N (2,1) demonstrated the most effective friction reduction, with its tribological properties in synergy with PG surpassing those of LCG.

4. Conclusions

This study systematically investigated the friction and wear performance of polyurea grease/lithium complex grease with various proportions of erucamide and N-phenyl- α -

naphthylamine additives. The findings were validated through bearing friction torque tests. Based on the results of this study, the following conclusions can be drawn:

- (1) The addition of erucamide to polyurea grease/lithium complex grease demonstrated a notable friction reduction effect, while the inclusion of N-phenyl- α -naphthylamine yielded a modest and indirect reduction in friction. When a combination of 2 wt. % erucamide and 1 wt. % N-phenyl- α -naphthylamine was employed, the combined effect of erucamide and N-phenyl- α -naphthylamine resulted in the optimal friction reduction. This combination performed exceptionally well in conjunction with polyurea grease, exhibiting superior tribological properties.
- (2) The polyurea thickener comprised a lamellar thickener composed of short rod-shaped fibers, with the base oil, erucamide, and N-phenyl- α -naphthylamine molecules dispersed within the thickener. In contrast, the lithium complex thickener was structured as a network of intertwined fibers, with the base oil adsorbed within, while erucamide and N-phenyl- α -naphthylamine molecules were distributed on the surface of the thickener.
- (3) In the friction torque tests, it was observed that when 3 wt. % erucamide was utilized, the starting torque was minimized. However, when a combination of 2 wt. % erucamide and 1 wt. % N-phenyl- α -naphthylamine was employed, the dynamic torque was minimized.
- (4) Considering the tribological properties and bearing friction torque performance, the polyurea grease containing erucamide and N-phenyl- α -naphthylamine showed promising lubrication properties, warranting further research and optimization. By using the test method in this paper, the ratios of erucamide and N-phenyl- α -naphthylamine were further optimized, testing concentrations such as 1.6%, 1.8%, 2.2%, 2.4%, etc., so as to obtain the optimal ratios of erucamide and N-phenyl- α -naphthylamine in polyurea grease.
- (5) The results of this study support that erucamide and N-phenyl- α -naphthylamine added to grease act on roller bearings with excellent tribological properties. In addition, there are limitations in the friction reduction effect of ER and N. The friction reduction effect of erucamide and N-phenyl- α -naphthylamine is limited to that seen for the greases prepared in this paper.

Author Contributions: The corresponding author is responsible for ensuring that the descriptions are accurate and agreed by all authors. Q.L.: Investigation, Validation, Data curation, Writing—original. Y.M.: Conceptualization, Methodology, Supervision. J.L.: Writing—review and editing. H.Z.: Validation, Investigation. All authors have read and agreed to the published version of the manuscript.

Funding: This research received no external funding.

Data Availability Statement: Data are contained within the article.

Conflicts of Interest: Authors Juncheng Lv and Hong Zhang were employed by the company SAIC GM Wuling Automobile Co., Ltd. The remaining authors declare that the research was conducted in the absence of any commercial or financial relationships that could be construed as a potential conflict of interest.

References

1. Wu, C.; Liu, Z.; Zhao, H.J.; Yang, H.N.; Li, X.L. Effect of the grease thickener on tribological properties of Si₃N₄/GCr15 contact interface and the performance in hybrid ceramic ball bearing. *Ceram. Int.* **2023**, *49*, 16857–16867. [[CrossRef](#)]
2. Liu, J.; Xu, Z.D. An optimization design method of a cylindrical roller bearing with the low friction torque. *J. Tribol. Trans. ASME* **2022**, *144*, 111201. [[CrossRef](#)]
3. Liu, Y.W.; Fan, X.Y.; Wang, J.; Liu, X.Y. An Investigation for the Friction Torque of a Tapered Roller Bearing Considering the Geometric Homogeneity of Rollers. *Lubricants* **2022**, *10*, 154. [[CrossRef](#)]
4. Gimeno, S.; Mescheder, H.; Quintana, I.; Gasi3n, A.; Arias-Egido, E.; Carbonell, A.; Mallo, C.; Miguel, I.; Paredes, J.; Zalakain, I. Effect of different laser texturing patterns on rolling contact surface and its tribological & fatigue life behavior on 100Cr6 bearing steel. *Wear* **2023**, *522*, 204717. [[CrossRef](#)]
5. Wingertzahn, P.; Koch, O.; Maccioni, L.; Concli, F.; Sauer, B. Predicting Friction of Tapered Roller Bearings with Detailed Multi-Body Simulation Models. *Lubricants* **2023**, *11*, 369. [[CrossRef](#)]

6. Farré-Lladós, J.; Westerberg, L.G.; Casals-Terré, J.; Leckner, J.; Westbroek, R. On the Flow Dynamics of Polymer Greases. *Lubricants* **2022**, *10*, 66. [[CrossRef](#)]
7. Lugt, P.M.; Berens, F. The Grease Life Factor concept for ball bearings. *Tribol. Int.* **2022**, *169*, 107460. [[CrossRef](#)]
8. Zhang, E.H.; Li, W.M.; Zhao, G.Q.; Wang, Z.; Wang, X.B. A study on microstructure, friction and rheology of four lithium greases formulated with four different base oils. *Tribol. Lett.* **2021**, *69*, 98. [[CrossRef](#)]
9. Biazon, L.; Ferrer, B.P.; Toro, A.; Cousseau, T. Correlations between rail grease formulation and friction, wear and RCF of a wheel/rail tribological pair. *Tribol. Int.* **2021**, *153*, 106566. [[CrossRef](#)]
10. Wang, Y.S.; Zhang, P.; Gao, X.D.; Cheng, Y.J. Rheological and tribological properties of polyurea greases containing additives of MoDDP and PB. *Tribol. Int.* **2023**, *180*, 108291. [[CrossRef](#)]
11. Xia, Y.Q.; Yang, K.; Feng, X.; Wang, Y.H. Tribological properties of modified kaolin doped polymer as polytetrafluoroethylene grease additive. *Tribol. Int.* **2022**, *173*, 107612. [[CrossRef](#)]
12. Kunishima, T.; Nagai, S.; Kurokawa, T.; Galipaud, J.; Guillonnet, G.; Bouvard, G.; Abry, J.C.; Minfray, C.; Fridrici, V.; Kapsa, P. Effects of temperature and addition of zinc carboxylate to grease on the tribological properties of PA66 in contact with carbon steel. *Tribol. Int.* **2021**, *153*, 106578. [[CrossRef](#)]
13. Bas, H.; Özen, O.; Besirbeyoglu, M.A. Tribological properties of MoS₂ and CaF₂ particles as grease additives on the performance of block-on-ring surface contact. *Tribol. Int.* **2022**, *168*, 107433. [[CrossRef](#)]
14. Padgurskas, J.; Johns, E.I.; Radulescu, I.; Radulescu, A.V.; Alexandru, V.; Rukuiz, R.; Snitka, V.; Kreivaitis, R.; Kupc, A.; Volskis, D. Tribological study of beeswax-thickened biogrease and its modification with carbon nanoparticles. *Tribol. Int.* **2023**, *184*, 108465. [[CrossRef](#)]
15. Xie, M.X.; Pan, B.L.; Liu, H.Y.; Li, N.; Chen, Z.; Yan, J.J.; Fu, Z.H.; Guo, S.H.; Wang, H.G. One-step synthesis of carbon sphere@1 T-MoS₂ towards superior antiwear and lubricity. *Tribol. Int.* **2022**, *176*, 107927. [[CrossRef](#)]
16. Wang, J.; Li, Z.P.; Zhao, H.; Ren, S.Z.; Wang, C.C.; Huang, X.F.; Zheng, L.; Ren, T.H. Synergistic effects between sulfur- and phosphorus-free organic molybdenums and ZDDP as lubricating additives in PAO6. *Tribol. Int.* **2021**, *165*, 107324. [[CrossRef](#)]
17. Wang, H.; Sun, A.N.; Qi, X.W.; Dong, Y.; Fan, B.L. Wear properties of textured lubricant films filled with graphite and polytetrafluoroethylene (PTFE) via laser surface texturing (LST). *Tribol. Int.* **2022**, *176*, 107414. [[CrossRef](#)]
18. Huang, Y.J.; Xiong, Y.C.; Liu, C.J.; Li, L.L.; Xu, D.Y.; Lin, Y.H.; Nan, C.W. Single-crystalline 2D erucamide with low friction and enhanced thermal conductivity. *Colloids Surf. A Physicochem. Eng. Asp.* **2018**, *540*, 29–35. [[CrossRef](#)]
19. Mansha, M.; Gauthier, C.; Gerard, P.; Schirrer, R. The effect of plasticization by fatty acid amides on the scratch resistance of PMMA. *Wear* **2011**, *271*, 671–679. [[CrossRef](#)]
20. Silvano, J.D.; Santa, R.A.A.B.; Martins, M.A.P.M.; Riella, H.G.; Soares, C.; Fiori, M.A. Nanocomposite of erucamide-clay applied for the control of friction coefficient in surfaces of LLDPE. *Polym. Test.* **2018**, *67*, 1–6. [[CrossRef](#)]
21. Jia, T.Y.; Tian, H.C.; Liu, S.T.; Zhang, S.J.; Ning, N.Y.; Yu, B.; Tian, M. Erucamide/thermoplastic polyurethane blend with low coefficient of friction, high elasticity and good mechanical properties for intelligent wearable devices. *Polym. Int.* **2023**, *72*, 813–821. [[CrossRef](#)]
22. Velázquez, J.D.H.; Barroso-Flores, J.; Goicochea, A.G. Ab initio modeling of friction reducing agents shows quantum mechanical interactions can have macroscopic manifestation. *J. Phys. Chem. A* **2016**, *120*, 9244–9248. [[CrossRef](#)] [[PubMed](#)]
23. Di, Y.Y.; Zhang, S.; Feng, X.Q.; Li, Q.Y. Tuning frictional properties of molecularly thin erucamide films through controlled self-assembling. *Acta Mech. Sin.* **2021**, *37*, 1041–1049. [[CrossRef](#)]
24. Gubala, D.; Taylor, N.; Harniman, R.; Rawle, J.; Hussain, H.; Robles, E.; Chen, M.; Briscoe, W.H. Structure, nanomechanical properties, and wettability of organized erucamide layers on a polypropylene surface. *Langmuir* **2021**, *37*, 6521–6532. [[CrossRef](#)] [[PubMed](#)]
25. Gubala, D.; Fox, L.J.; Harniman, R.; Hussain, H.; Robles, E.; Chen, M. Heads or tails: Nanostructure and molecular orientations in organised erucamide surface layers. *J. Colloid Interface Sci.* **2021**, *590*, 506–517. [[CrossRef](#)] [[PubMed](#)]
26. Liu, Q.C.; Mo, Y.M. Effect of erucamide as polyurea grease additive on tribological properties of GCr15 steel. *Tribol. Trans.* **2023**, *66*, 507–518. [[CrossRef](#)]
27. He, Z.Y.; Xiong, L.P.; Liu, J.; Han, S.; Hu, J.Q.; Xu, X.; Shen, M.X. Tribological property study of mercaptobenzothiazole-containing borate derivatives and its synergistic antioxidative effects with N-phenyl- α -naphthylamine. *Lubr. Sci.* **2019**, *31*, 239–251. [[CrossRef](#)]
28. Xiong, L.P.; He, Z.Y.; Liu, J.; Hu, J.Q.; Han, S.; Wu, Y.L.; Yang, S.M. Tribological study of N-containing borate derivatives and their synergistic antioxidation effects with T531. *Friction* **2019**, *7*, 417–431. [[CrossRef](#)]
29. Hu, J.Q.; Wei, X.Y.; Yao, J.B.; Han, L.; Zong, Z.M. Evaluation of molybdate ester as a synergist for arylamine antioxidant in lubricants. *Tribol. Int.* **2006**, *39*, 1469–1473. [[CrossRef](#)]
30. Wang, S.P.; Yu, S.S.; Huang, B.; Feng, J.X.; Liu, S.G. Unique synergism between zinc dialkyldithiophosphates and Schiff base bridged phenolic diphenylamine antioxidants. *Tribol. Int.* **2019**, *145*, 106134. [[CrossRef](#)]
31. Jiang, C.; Wang, Y.N.; Su, H.G.; Li, W.M.; Lou, W.J.; Wang, X.B. Synthesis and evaluation of a protic ionic liquid as a multifunctional lubricant additive. *Friction* **2020**, *8*, 568–576. [[CrossRef](#)]
32. Duangkaewmanee, S.; Petsom, A. Synergistic and antagonistic effects on oxidation stability of antioxidants in a synthetic ester-based oil. *Tribol. Int.* **2011**, *44*, 266–271. [[CrossRef](#)]

33. Joly, J.F.; Miller, R.E. Density functional theory rate calculation of hydrogen abstraction reactions of N-Phenyl- α -naphthylamine antioxidants. *Ind. Eng. Chem. Res.* **2018**, *57*, 876–880. [[CrossRef](#)]
34. Ma, R.; Li, W.M.; Zhao, Q.; Zheng, D.D.; Wang, X.B. In situ synthesized phosphate-based ionic liquids as high-performance lubricant additives. *Tribol. Lett.* **2019**, *67*, 60. [[CrossRef](#)]
35. He, Z.Y.; Xiong, L.P.; Han, S.; Chen, A.X.; Qiu, J.W.; Fu, X.S. Tribological and antioxidation synergistic effect study of sulfonate-modified nano calcium carbonate. *PLoS ONE* **2013**, *8*, e62050. [[CrossRef](#)]
36. *GB/T 32562-2016*; Rolling Bearings-Measuring Methods for Friction Torque. China Machinery Industry Federation: Beijing, China, 2016.
37. Xue, Y.W.; Wu, C.H.; Shi, X.L.; Zhang, K.P.; Huang, Q.P. High temperature tribological behavior of textured CSS-42L bearing steel filled with Sn-Ag-Cu-Ti₃C₂. *Tribol. Int.* **2021**, *164*, 107205. [[CrossRef](#)]
38. Dulal, N.; Shanks, R.; Chalmers, D.; Adhikari, B.; Gill, H. Migration and performance of erucamide slip additive in high-density polyethylene bottle caps. *J. Appl. Polym. Sci.* **2018**, *153*, 46822. [[CrossRef](#)]

Disclaimer/Publisher's Note: The statements, opinions and data contained in all publications are solely those of the individual author(s) and contributor(s) and not of MDPI and/or the editor(s). MDPI and/or the editor(s) disclaim responsibility for any injury to people or property resulting from any ideas, methods, instructions or products referred to in the content.